Manuscript Details

Manuscript number	CAGEO_2017_297
Title	PAF: A software tool to estimate free-geometry extended bodies of anomalous pressure from surface deformation data
Article type	Research Paper

Abstract

We present a software package, namely PAF, to carry out inversions of surface deformation data (any combination of InSAR, GPS, and terrestrial data) as produced by 3D free-geometry extended bodies with anomalous pressure changes. The anomalous structures are described as aggregation of elementary cells (point sources) in an elastic half space. The linear inverse problem (supply with some simple regularization conditions) is solved by means of an exploratory approach. This software represents the open implementation of a previously published methodology. It can be freely downloaded from the journal web page or asked to the corresponding author, and used both with large data sets (e.g. InSAR data sets) or with data coming from small control networks (e.g. GPS monitoring data), mainly in volcanic areas to estimate the expected causative pressure bodies. Here, PAF software is applied to some real test cases.

Keywords	software, surface deformation, pressure sources, volcano monitoring
Taxonomy	Volcanology, Modelling
Manuscript category	Surveying and monitoring
Corresponding Author	Jose Fernandez
Corresponding Author's Institution	CSIC
Order of Authors	Antonio G. Camacho, Jose Fernandez, Flavio Cannavo
Suggested reviewers	Kristy Tiampo, Pietro Tizzani, Maurizio Battaglia

Submission Files Included in this PDF

File Name [File Type]

Cover_letter_27-03-2017.docx [Cover Letter]

Camacho_et_al_PAF-Sofware.pdf [Manuscript File]

To view all the submission files, including those not included in the PDF, click on the manuscript title on your EVISE Homepage, then click 'Download zip file'.

Dear Editor:

Please find attached the manuscript "PAF: A software tool to estimate free-geometry extended bodies of anomalous pressure from surface deformation data." by A.G. Camacho, J. Fernández and F. Cannavó, we would like to publish in Computers & Geosciences journal.

It is a re-submission of the manuscript CAGEO_2017_158, after providing in the text where the source code of the software can be found, under an open source license. The source codes are also available for reviewers if they need. See last sentence of conclusions The editor who managed the previous manuscript was Prof. Edzer Pebesma.

The manuscript have been not submitted for consideration to any other journal.

Yours,

José Fernández

Correponding author

PAF: A software tool to estimate free-geometry extended bodies of anomalous pressure from surface deformation data.

A.G. Camacho [1], J. Fernández [1,*], F. Cannavó [2]

[1] Institute of Geosciences (CSIC-UCM), Madrid, Spain

[2] Osservatorio Etneo, Istituto Nazionale di Geofisica e Vulcanologia, Catania, Italy.

_____

*Corresponding author:

Institute of Geosciences (CSIC-UCM), Fac. C. Matemáticas, Plaza de Ciencias, 3. 28040-Madrid.

Spain. e-mail: jft@mat.ucm.es; phone: +34-913944632

Abstract: We present a software package, namely PAF, to carry out inversions of surface deformation data (any combination of InSAR, GPS, and terrestrial data) as produced by 3D free-geometry extended bodies with anomalous pressure changes. The anomalous structures are described as aggregation of elementary cells (point sources) in an elastic half space. The linear inverse problem (supply with some simple regularization conditions) is solved by means of an exploratory approach. This software represents the open implementation of a previously published methodology. It can be freely downloaded from the journal web page or asked to the corresponding author, and used both with large data sets (e.g. InSAR data sets) or with data coming from small control networks (e.g. GPS monitoring data), mainly in volcanic areas to estimate the expected causative pressure bodies. Here, PAF software is applied to some real test cases.

1. Introduction.

In a volcanic context, surface deformation data are normally inverted to infer information about the intrusive pressure sources (e.g., Rymer and Williams-Jones, 2000; Dzurisin, 2003). The surface deformation is related to the dynamics of volcanic plumbing systems, such as the shape of magma intrusions, magma pressure, and emplacement mechanisms. Normally, regular geometries (point sources, disks, prolate or oblate spheroids, etc.) are assumed at the initial stages (Lisowski, 2007). The inversion approach for the deformation data is usually based on the hypothesis of spherical, ellipsoidal or general extended causative bodies. Other types of analytical models, as fault, dike, laminar or cylindrical structures, are sometimes employed. Moreover, the mathematical model for the source structure must consider some elastic properties to account for the deformation phenomena. Usual analytical modeling assumes an elastic, homogeneous and isotropic crust, but it can take into account effects from several source geometries, topography relief and gravity background (Williams and Wadge, 1998; Charco et al., 2007; Battaglia and Hill, 2009).

Camacho et al. (2011) presented an original methodology for simultaneous inversion of vertical (Up), east-west (EW), and north-south (NS) deformation components and/or LOS InSAR displacement, by means of 3D extended bodies, with free geometry, for anomalous pressure. Assuming homogenous elastic conditions, the approach determines a general geometrical configuration of pressurized sources corresponding to prescribed values of anomalous pressure. The sources are described as an aggregate of pressure point sources, and they fit the entire data within some regularity conditions. The approach works in a step-by-step growth process that allows retrieving very general geometrical configurations.

This approach provides interesting results for volcanic areas (Camacho et al., 2011; Samsonov et al., 2014; and Cannavó et al., 2015b) when deformations come from pressure sources. The subsurface volume is divided into a 3D partition of (thousands) elemental cells. The aggregation of elemental

47 sources (with superposition of their strain contribution) forms the geometry of the extended causative

48 bodies.

49   The observation equations are [see Camacho et al. (2011) for a detailed description]:

$$ds = ds^{c} + v \qquad (1)$$

51 where ds, ds^{c} represent the vector of observed and calculated three component (3D) of the

52 displacement, and v is the vector for residual values coming from uncertainties in the observation

53 process and the imperfect model fit.

54   The surface deformations, ds^{c}, due to a buried over pressure structure are calculated as the

55 aggregated effect of different point sources, as due to the deformation effects from the incremental

56 pressure p_k and expansion radius within the elastic semi space, described by the Mogi model (Mogi,

57 1958; Rymer and Williams-Jones, 2000).

58   The inversion equations are solved by means of adding a regularization condition:

$$v^{T} Q_{D}^{-1} v + \lambda\, m^{T} Q_{M}^{-1} m = \min . \qquad (2)$$

60 where model vector m is constituted by the pressure values p_k, $k=1,...,m$, for the m cells of the model,

61 Q_D is the covariance matrix of data, Q_M is a suitable covariance matrix corresponding to the physical

62 configuration and λ is a smoothing factor that balances the goodness of fit and smoothness of the

63 model. The inversion approach is a non-linear problem.

64   The final source is determined as a free aggregation of a large number of small over (under)

65 pressured sources. The inversion algorithm carries out a step-by-step process of growth of the 3D

66 models, using an exploratory technique to sequentially find the new cell/point source to be set as

67 (de)pressurized and aggregated to the model to improve the fit to the data (Camacho et al., 2011).

68   In fact, at the k-th step of the growth process, k cells are filled with the prescribed anomalous values

69   for pressure, giving rise to the modelled values ds^c. Successively, at the new $(k+1)$-th step, the

70   algorithm searches for a new cell to fill to improve the fit following the system:

71    $$\mathbf{ds} = f\,\mathbf{ds}^c + \mathbf{v} \tag{3}$$

72    $$\mathit{misfit} = \mathbf{v}^T \mathbf{Q}_D^{-1} \mathbf{v} + \lambda\, f^2 \mathbf{m}^T\, \mathbf{Q}_M^{-1}\, \mathbf{m}\,, \tag{4}$$

73   where $f>1$ is a scale factor, estimated during the inversion, to allow for a fit between the anomaly of

74   the provisional model and the observed anomaly.

75   This inversion methodology has been tested by means of several synthetic tests (Camacho et al,

76   2011), and also by real application to volcanic environments: Campi Flegrei (Italy) (Camacho et al,

77   2011; Samsonov et al., 2014) and Mount Etna (Italy) (Cannavo et al, 2015b).

78   In the next section, we describe the proposed software tool (PAF-package) that allows for a simple

79   and nearly automatic application of this methodology. Then, we present two real applications that

80   illustrate the selection of parameters and some features of the adjusted model for over pressure bodies.

81   Most of the following figures are created by the PAF software.

82   **2. The PAF Software.**

83   The software package consists of two executable files: **ConfigPAF.exe** and **InverPAF.exe**. The

84   first one determines a 3D partition of the subsurface volume into a grid of small parallelepiped cells

85   through a graphical interface for the input of the inversion parameters. It creates an intermediate file

86   (**CellsConfig.txt**) with the information of cell partitions. The second one, **InverPAF.exe**, reads the

87   displacement data and the intermediate file (**CellsConfig.txt**), and runs the inversion to model the

88   observed data with some 3D extended bodies of anomalous pressure described as aggregation of filled

89   cells.

90   The PAF software can work in two different ways: (1) statically, considering large displacement

91 data files describing the deformation field (for instance, thousands of pixels with displacement values

92 from SAR interferometry, or combined with GPS data) for a concrete time period; and (2) dynamically,

93 sequential inversion of successive stages of a deformation process (for instance, successive GPS

94 displacement data obtained at different epochs from a permanent monitoring network).

95 **2.1.Input files and data.**

96   The 3D deformation data from the several sites are collected in the file **DeforData.txt**. This file

97 contains, for each data point, coordinates UTM East-North (m), altitude (m), and deformation values

98 dz (cm, positive upward), dx (cm, positive eastward) and dy (cm, positive northward). The value in the

99 adjacent column, associated to each measurement, indicates whether the corresponding deformation

100 value has to be included in the inversion process (one) or not (zero). This data file can optionally be

101 terminated with an end-of-file character or with a line of zeros.

102   A secondary data file is **map.bln**, which can be optionally used to draw the cartography of the

103 studied area. It includes numerical values of polygonal lines (described by the coordinates of the

104 vertexes) with topographical details (roads, etc.).

105   In the case of sequential application, the successive data are provided on successive files, named

106 **Dn.txt**, where n is a successive integer number, and with the same format as **DeforData.txt**.

107 **2.2.Software Usage.**

108   Once the data are available, the first step to perform an inversion with PAF is to generate a suitable

109 3D partition of the subsurface volume into a grid of small parallelepiped cells. This step is carried out

110 by using the **ConfigPAF.exe** tool. This program reads the data in **DeforData.txt** (Figure 1) and sets

111 several parameters by means of a friendly dialog window (Figure 2), offering default values.

112

```
425575 4527988    91.6    0.38   1   -0.23   1     0  0
425844 4527985    95.7    0.37   1   -1.53   1     0  0
426114 4527982   105.0    0.94   1   -0.21   1     0  0
426383 4527980   102.7    0.02   1   -0.48   1     0  0
425103 4527948    90.7    1.72   1    1.80   1     0  0
426653 4527932   111.6    0.95   1   -0.86   1     0  0
426922 4527930   130.7    1.56   1    0.52   1     0  0
424799 4527907    97.7    0.40   1   -1.91   1     0  0
427191 4527883   132.0    0.37   1    0.86   1     0  0
425338 4527857    85.9    0.55   1    1.08   1     0  0
427460 4527835   154.1    1.04   1    0.09   1     0  0
424326 4527822    80.8    0.94   1    0.32   1     0  0
```

Figure 1. Input data file DeforData.txt containing coordinates UTM (m), altitude (m), and deformation values dz (cm), dx (cm) and dy (cm) for the data points. Values of 0 and 1 are used to indicate whether the values are included or not, respectively.

Figure 2. Input dialog window for the parameters of the 3D grid of cells to prepare the inversion calculus.

In the upper part of the Graphical User Interface (GUI) (Figure 2), the user can revise the default values for the geometrical parameters of the partition: depth (m above sea level) of the top of the
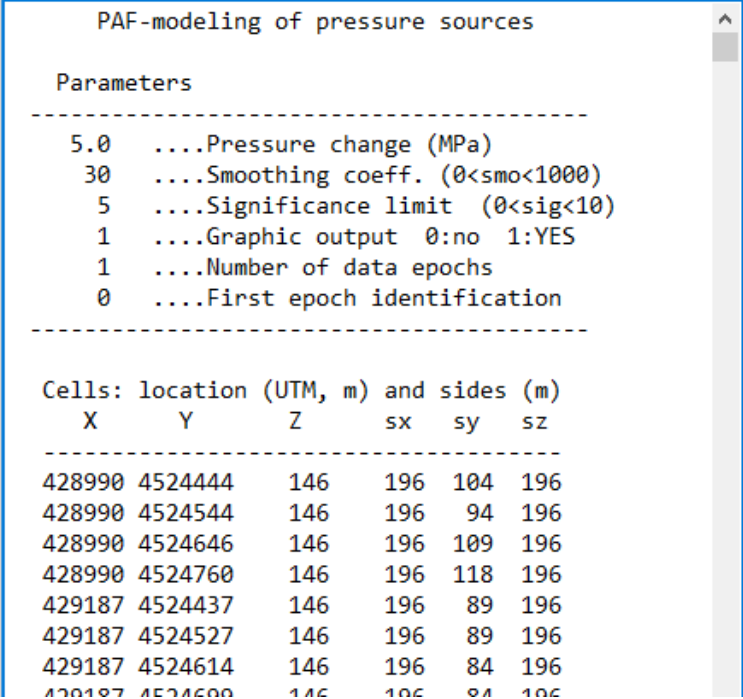
6

122   partition volume, depth (m, above sea level) of the bottom of the partition volume, and mean side size

123   (m) of the cells. Once these values are set (pressing Run/OK), the program calculates the resulting

124   number of cells.

125   Then, in the bottom part of the GUI (Figure 2), the program requires two more parameters: (a) the

126   dimensionless smoothing coefficient λ (ranging between 0 and 1000), and, (b) a value for the (positive

127   or negative) pressure contrast throughout the entire anomalous model, Δp (MPa). The λ coefficient

128   regulates the balance between data fit and model complexity in the inversion approach. For a low λ

129   value (close to 0) the resulting model becomes very simple, regular and compact, but the data fit can

130   be weak. Conversely, a high λ value (close to 1000) the data fit is very good (even by fitting some

131   noise component), but the resulting model can be very complex, sometimes even with artefacts. We

132   have imagined some objective criterion (see for instance, Camacho et al. 2007, in other context), but

133   for practical applications, we suggest to try different values in a trial and error manner, and to select

134   the most appropriate one considering the resulting models. Some criteria for choosing this value are:

135   be sure that the program finishes the inversion (for too high or too low values of the parameter, the fit

136   conditions are invalid and the program stops); auto-correlated components or significant signal in the

137   residuals should be avoided; the resulting model should be regular and simple (avoiding very small

138   and sparse shallow body for noise inversion). For more details, see the two application examples

139   below.

140   The pressure contrast value Δp can be selected trial and error also by doing some iterative running

141   of the software. For very high values, the model becomes very condensed and compact, and some

142   geometrical details can be lost. Conversely, for very low values the sources model becomes larger,

143   with rounding inflated shape. In general, big displacements require strong pressure contrasts and small

144   ones require low-pressure contrasts. We suggest, again, some iteration trying different values and

145   observing the resulting anomalous geometry. Nevertheless, this is not a critical parameter. It concerns

146   mostly to rather aesthetic aspects of the model. See also application examples below.

7

147   Once the **ConfigPAF.exe** is completed (by pressing Run/OK), it creates a new file, namely

148   **CellsConfig.txt**. This is an intermediate file containing (see Figure 3): (a) the assumed values for the

149   inversion parameters (smoothing coefficient, pressure contrast, etc.), and (b) the geometrical

150   parameters (location and sides) of the parallelepiped cells.

151


```
        PAF-modeling of pressure sources

     Parameters
    -----------------------------------------
      5.0    ....Pressure change (MPa)
       30    ....Smoothing coeff. (0<smo<1000)
        5    ....Significance limit  (0<sig<10)
        1    ....Graphic output  0:no  1:YES
        1    ....Number of data epochs
        0    ....First epoch identification
    -----------------------------------------


     Cells: location (UTM, m) and sides (m)
        X      Y       Z     sx   sy   sz
    -----------------------------------------
     428990 4524444   146   196  104  196
     428990 4524544   146   196   94  196
     428990 4524646   146   196  109  196
     428990 4524760   146   196  118  196
     429187 4524437   146   196   89  196
     429187 4524527   146   196   89  196
     429187 4524614   146   196   84  196
     429187 4524699   146   196   84  196
```

152   ***Figure 3.*** *Intermediate file CellsConfig.txt containing the assumed values for the inversion*

153   *parameters, and the geometrical parameters (location and sides) of the parallelepiped cells.*

154   The values of the parameters contained in this file can be manually modified to adapt to the

155   modeller necessities. For instance, the third parameter, "*Significance limit (0<sig<10)*", gives the

156   desired threshold between the significant cells (for those close and covered by the data points) from

157   the non-significant cells (for those far from the data points). Its default value is 5, but the user can set

158   optionally a different value (for instance, for a low significance threshold, nearly all cells will be

159   considered as significant). The fourth parameter ("*Graphic output 0:no 1:YES*") is used to switch the

8

160 graphical output during the inversion approach (see below the content of this graphical output). The

161 fifth parameter indicates that the data correspond to only one epoch, or conversely that the inversion

162 has to be carried out in a sequential process of a number of epochs, starting at the epoch and with the

163 data file identified by the sixth parameter.

164

165

166

167
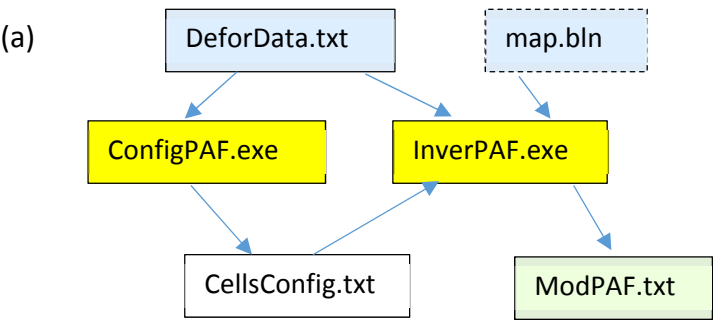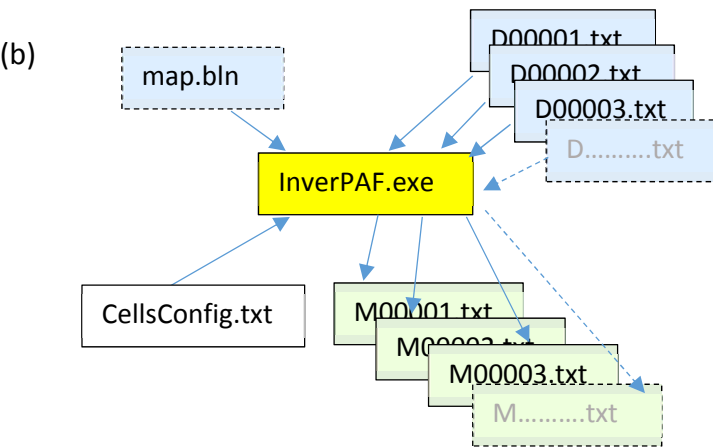
168 **Figure 4.** *Scheme of the application of the PAF software. (a) Case of deformation data for one epoch*

169 *(for instance, thousands of pixel for a SAR interferogram), (b) Sequential application of the inverse*

170 *approach for successive data files (in blue) producing successive model files (in green) and graphic*

171 *pictures (case of a monitoring network)*

172   Once the file **CellsConfig.txt** is created (and optionally revised), the inversion approach by

173   **InverPAF.exe** can start (Figure 4). It runs automatically, without any other requirement, and produce

174   an optional visualization (fourth parameter in CellCnfig.txt) of the inversion process and of the results

175   on the screen. In the case of sequential application (Figure 4b), the **InverPAF.exe** process works

176   continuously, epoch by epoch, until it inverts the data of the last epoch. As final product, the inversion

177   approach creates an output file named **ModPAF.txt** containing the geometrical description of the

178   resulting model, several others parameters of this model, and a detailed information about modelled

179   and residual values. They will be described further on.

180   **2.3. Output files and pictures**.

181   Figure 5 shows an example of the graphical output that can be optionally displayed throughout the

182   inversion approach (see Figure 4 and corresponding description text). This visual information contains

183   some interesting graphics about the model growth process and about the final results. Statistics about

184   the model growth process are: *misfit* value (see equation 4) evolution, pressure value evolution, planar

185   and vertical cuts views (EW and NS) of the aggregation process (significant cells in red and dark blue,

186   no significant cells in yellow and light blue, cells of a previous epoch in green), observed and modelled

187   deformations (along EW and along NS), inversion parameters (step number, pressure value, root mean

188   square (rms) residuals, cell depth). Statistics about the final results are: *misfit* value (equation 4),

189   number of rejected data, number of filled cells, and number of significant cells.
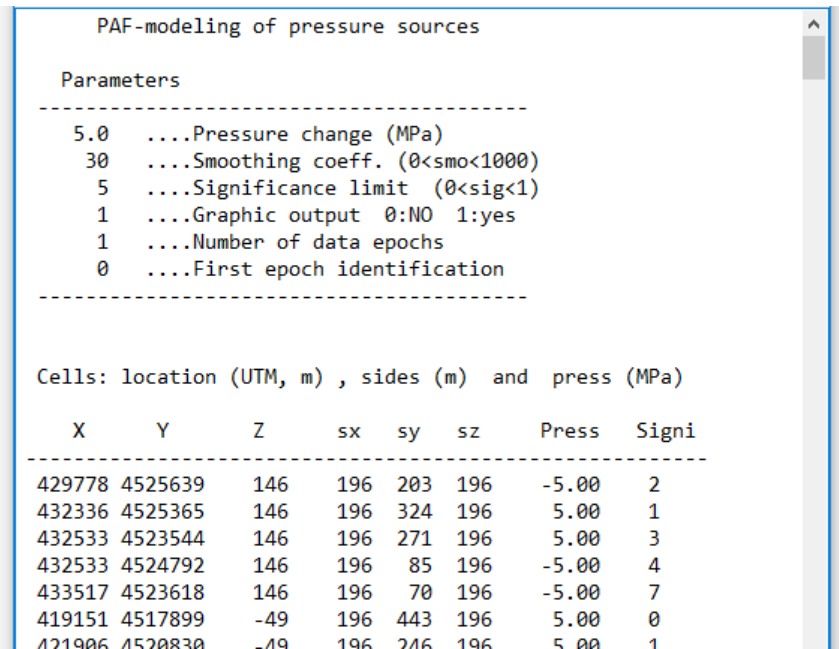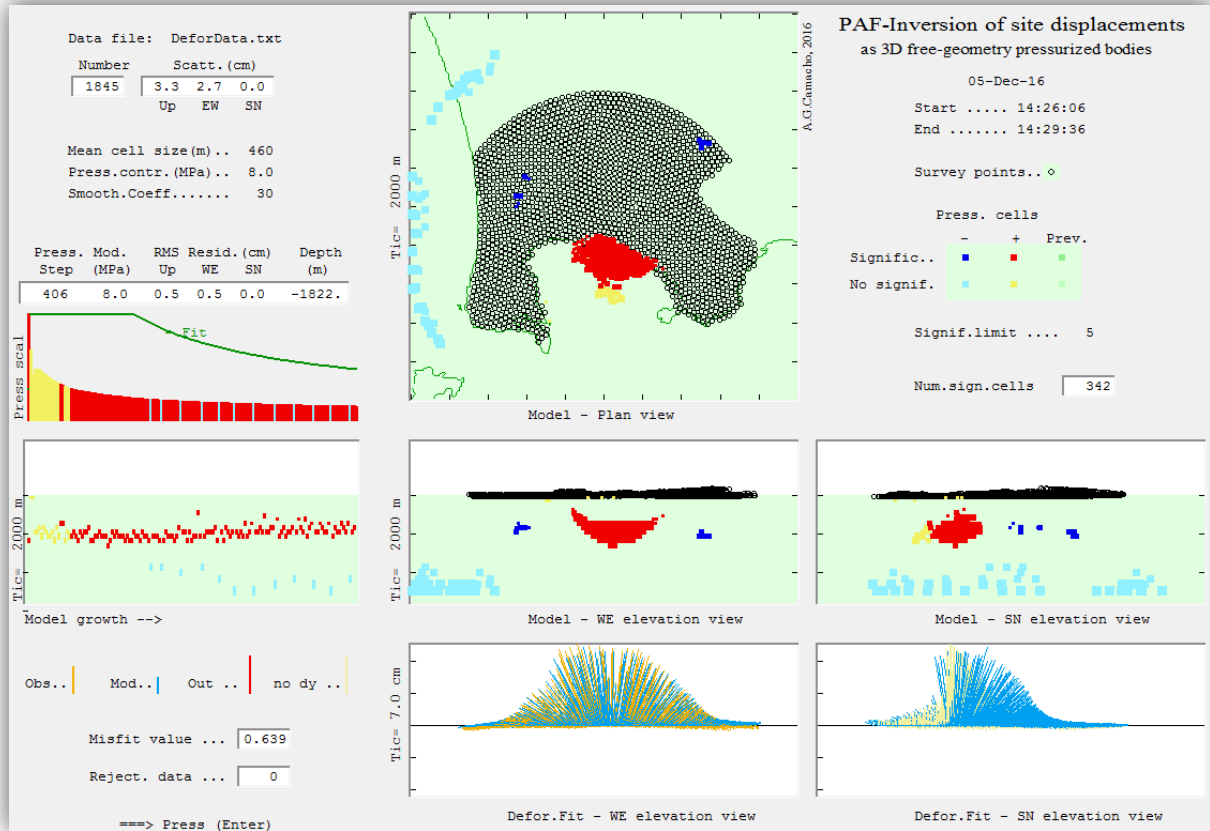
190

Figure 5. Example of the (optional) screen drawing along the inversion approach. It informs about the evolution of the model growth process and about some results.

The main product of the PAF inversion is the file **ModPAF.txt**. This file contains the following information:

(1) A copy of the assumed inversion parameters (Figure 6) similar to that in file **CellConfig.txt**.

(2) A list of the filled cells (those with no-null pressure values) containing (see Figure 6); for each cells, the UTM coordinates X and Y (m), and the depth Z (m, above sea level) of its geometric center, their sides sizes s_x ,s_y ,s_z (m), the corresponding positive or negative pressure contrast value, and a value for the significance (given by the inverse of the root mean square distance of the cell with respect

200 to the data points, normalized to range from 0 to 20). Higher values of significance correspond to more

201 sensitive cells. This part can be used for further, more sophisticated, drawings of the resulting model.

202

```
        PAF-modeling of pressure sources

     Parameters
    ----------------------------------------
     5.0    ....Pressure change (MPa)
      30    ....Smoothing coeff. (0<smo<1000)
       5    ....Significance limit  (0<sig<1)
       1    ....Graphic output  0:NO  1:yes
       1    ....Number of data epochs
       0    ....First epoch identification
    ----------------------------------------


   Cells: location (UTM, m) , sides (m)  and  press (MPa)

     X       Y       Z     sx   sy   sz    Press   Signi
    -----------------------------------------------------
   429778 4525639   146    196  203  196   -5.00    2
   432336 4525365   146    196  324  196    5.00    1
   432533 4523544   146    196  271  196    5.00    3
   432533 4524792   146    196   85  196   -5.00    4
   433517 4523618   146    196   70  196   -5.00    7
   419151 4517899   -49    196  443  196    5.00    0
   421906 4520830   -49    196  246  196    5.00    1
```

203 ***Figure 6.*** *Upper content of the output file **ModPAF.txt**. First, the modelling parameters are shown,*

204 *Then, the list of the filled cells (coordinates, sides, significance) are included.*

205 (3) After that, some additional parameters and results about the inversion process are given,

206 followed by a list of the observed, modelled and residual values for the data points (see Figure 7). For

207 each point, the file contains UTM coordinates (m), altitude (m), observed, modelled and residual values

208 (cm) for each component (*dz, dx, dy*), and an additional value for relative quality weighting (mean

209 value 1) according to the resulting residual values for the three components. This part of the output file

210 can be used for further drawings and statistical analysis of the inversion residuals (see examples

211 below).

212 In the case of sequential application of the PAF inversion approach, for each successive data file

213 **D…....txt** (e.g., **D00016.txt**) corresponding to successive monitoring epochs (respective sixteenth

12

214   epoch), the program generates a model file **M…….txt** (e.g., **M00016.txt**) with the same content as

215   **ModPAF.txt**.


```
421443 4532415  -6109    439 1277  439    -5.00   1
422763 4532598  -6109    439 1211  439    -5.00   1
437719 4527158  -6109    439 1277  439     5.00   1
-------------------- Date:08-Nov-16------------------

Num. data points =  1061
Num. total cells= 50599
Num.filled cells=  469    Neg, Pos =  160  309
Medium param.:      Poisson=0.25    Share Mod.= 10.GPa
Random explor.coeff.=  10
Pressure model:     Press. contrast (-+)=   5.00 MPa
                    Press*vol:  150.1 MPA*Km3    Mean mod.depth = -3875.
RMS residuals (cm): Up= 0.46    WE= 0.58    SN= 0.33    Misfit=   0.3390
Initial and final exec.times:   09:55:38    09:56:51



                Observed, modeled, and residual values

Data point loc(UTM, m)        dz (cm)          dx(cm)              dy(cm)
   X      Y      Z     obs  mod  res       obs   mod   res       obs mod res    Weight
----------------------------------------------------------------------------------
426261 4528962   96   -0.11 -0.74  0.63   -1.70 -1.50 -0.20     2.00  1.68  0.32   1.0
426611 4528958  102    0.27 -0.67  0.94   -1.60 -1.35 -0.25     2.00  1.62  0.38   0.2
425351 4528878   90    0.42 -1.01  1.43   -1.50 -2.09  0.59     1.60  1.69 -0.09   0.0
426960 4528862  111    0.50 -0.59  1.09   -1.00 -1.18  0.18     2.10  1.64  0.46   0.0
427309 4528859  110    0.01 -0.55  0.56   -2.10 -0.98 -1.12     2.10  1.64  0.46   1.0
425700 4528783   99    0.48 -0.79  1.27   -1.40 -1.93  0.53     2.10  1.95  0.15   0.0
426049 4528687  102    0.86 -0.63  1.49   -0.20 -1.42  1.22     2.50  2.00  0.50   0.0
426398 4528684  108    0.11 -0.65  0.76   -0.90 -1.39  0.49     2.20  1.79  0.41   0.8
```

216

217   ***Figure 7.*** *Last part content of the output file ModPAF.txt. Top: End of the list of the filled cells*

218   *(coordinates, sides, significance). Mean: Some parameters and results about the inversion process.*

219   *Bot: List of the observed, modelled and residual values (cm) for each data point.*

220   The code is in Fortran language and the executable compiled files are obtained with Microsoft

221   Visual Studio Community 2015 for Windows 10 64 bits operative system.

222   **3. Application examples**

223   **3.1.** *Campi Flegrei inflation case***.**

224   Campi Flegrei, one of the most hazardous volcanic areas in the world because of its close proximity

225   to the city of Naples, is the subject of many studies and surveys. Samsonov et al. (2014) apply the

13

226 multidimensional small baseline subset (MSBAS) differential interferometric synthetic aperture radar

227 (DInSAR) technique to obtain vertical (Up) and horizontal components (EW) of ground deformation

228 for Campi Flegrei at high spatial and temporal resolutions spanning along 20 years. Their results show

229 that the area underwent continuous subsidence from 1993 through 1999, followed by several alternate

230 periods, and a moderate uplift which began in 2007 and increased through 2012, reaching to about 17

231 cm by 2013. We study the uplift period from 2007/10/03 to 2013/06/15, taking as input data the

232 accumulated 2D deformation (Up and EW components).

233   From the thousands of pixels obtained by Samsonov et al. (2014) we have selected 1845 pixels

234 with mutual distance larger than 250 m and with a distance to the centre of deformation smaller than

235 8 km. Figure 8 shows the distribution of the selected pixels and the feature of the vertical component

236 (with more than 12 cm accumulated in the central area).

237   Once the 3D deformation data for the 1845 pixels is arranged in the file **DeforData.txt**, we can

238 apply the described process and software. The program **ConfigPAF.exe** suggests some default values:

239 437 m for altitude of the model top, -5915 m for depth of the model bottom, and 231 m for mean cell

240 side. We accept the first two values, but we try 180 m for mean cell side, looking for higher resolution.

241 For this new value, the resulting number of cells is 72017, as provided by the program.

242   Then, the program suggests the usual default values 200 for smoothing coefficient and 0.5 MPa for

243 pressure contrast. They are very general values. For this particular case of Campi Flegrei we have a

244 very strong accumulated deformation field, and it requires a higher pressure contrast. After some trials

245 we select 10.0 MPa (accumulated pressure for the anomalous volume elements) as tentative model

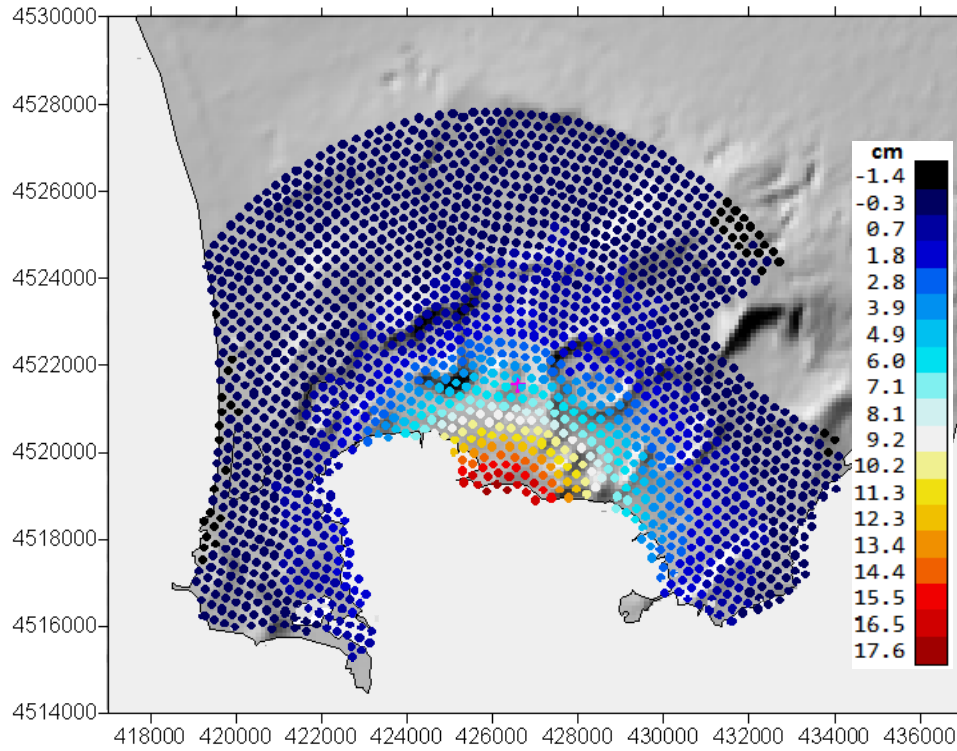246 contrast (for smaller values the anomalous structure becomes very inflated).

247

Figure 8. *Selected pixels and vertical deformation (cm) (annual linear rate) for an inflation episode in Campi Flegrei (Italy). UTM coordinates. Uplift period 10/2007-06/2013.*

About the smoothing coefficient λ, the general value 200 can be acceptable for usual cases. In this case of strong deformation, the signal/noise ratio is very high (see below, final residual level with respect to data scattering level), and the model does not require so high smoothing value. After some trials, we select 10 as suitable smoothing value. Nevertheless, the difference between models obtained with different inversion values is not critical (as a way of example, Figure 5 shows the model obtained with a value of 30 for smoothing and 8.0 MPa for accumulated pressure).

Once these values are selected, the rest of the inversion approach is nearly automatic. The number of epochs is one. We accept the general value 5 for the significance limit. Figure 9 shows the resulting model by means of planar and vertical cuts views. The model consists mostly of an anomalous body, at a mean depth about 1.8 km, composed of overpressure cells (red colour for significant cells and yellow for non-significant cells). Morphology of the anomalous structure as a "partially filled parabolic

15

261 glass" suggest a shallow (depth 1-2 km) hydrothermal system confined to the caldera fill materials.

262 This result is very similar to that obtained in Camacho et al. (2011) for the uplift period 1992-2000.
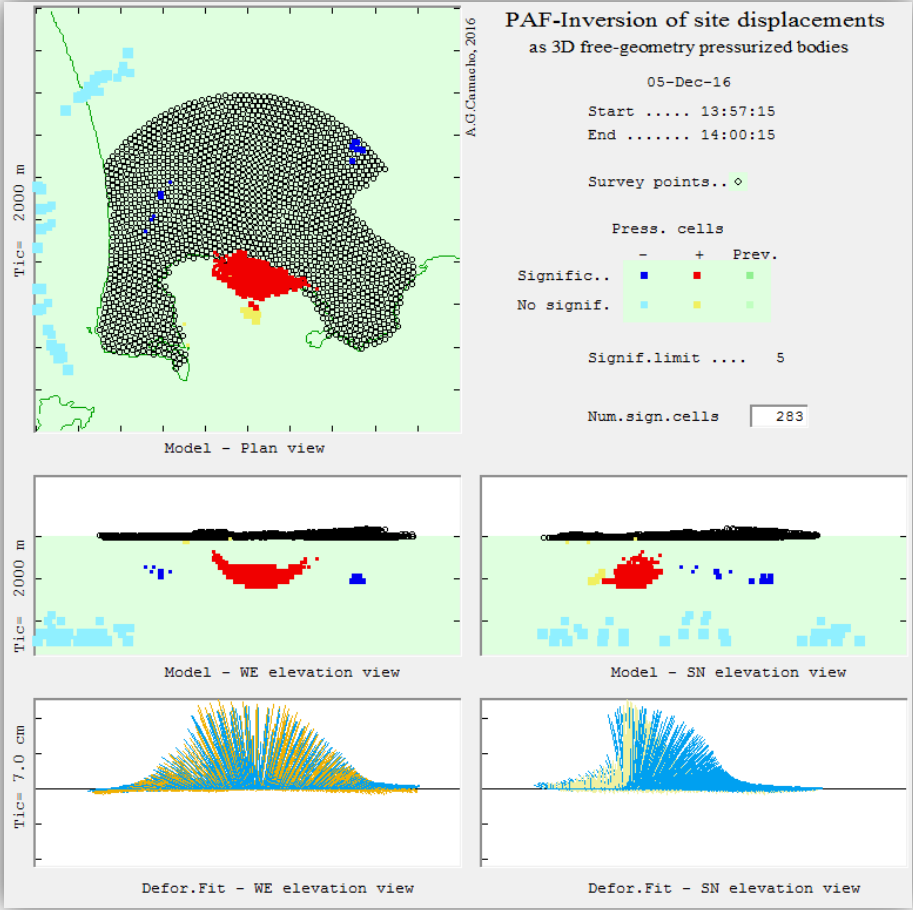
263

264 **_Figure 9._** _Resulting inversion model for the Campi Flegrei inflation data as subsurface anomalous_

265 _structure (about 1.8 km mean depth) of aggregated overpressure cells._

266   The final residual values after the inversion approach (root mean square values of 0.5 cm for Up,

267 and EW components) are quite small with respect to the total scattering of the deformation data (3.3

268 cm and 2.7 cm accumulated for Up and EW, respectively), confirming the suspected good ratio

269 signal/noise in the present deformation case.

270   Figure 9 also shows two vertical views of the fit between observed (orange lines) and modelled

271 (blue lines) deformations in the bottom. (Light yellow lines correspond to dz data without dy values,

16

272 the approach determines modelled values also for *dy*). In this figure, we can also observe the presence

273 of several areas with non-significant cells (light blue and yellow ones), mostly in peripheral areas.

274 These fictitious structures are introduced by the inverse approach to absorb distortion effects contained

275 in the interferometric data. These fictitious bodies allow for getting the significant structures nearly

276 free of distortion components in the data.

277 **3.2. *Etna monitoring case*.**

278   A second example regards the sequential application of the PAF software to a network of 31

279 permanent GPS stations close to Etna mountain (Sicily, Italy) (Cannavò et al., 2015b and references

280 on it), see Figure 10. Mt. Etna, situated on the eastern coast of Sicily, is a large basaltic volcano built

281 up in a geodynamic setting generated during the Neogene convergence between the African and

282 European plates (Allard et al., 2006; Branca et al., 2011) and is one of the most active volcanoes in the

283 world. Its activity comprises strombolian activity, which may evolve into lava fountains and effusive

284 events, and lateral eruptions occurring along fractures (Aloisi et al., 2006; Cannavò et al., 2015a).
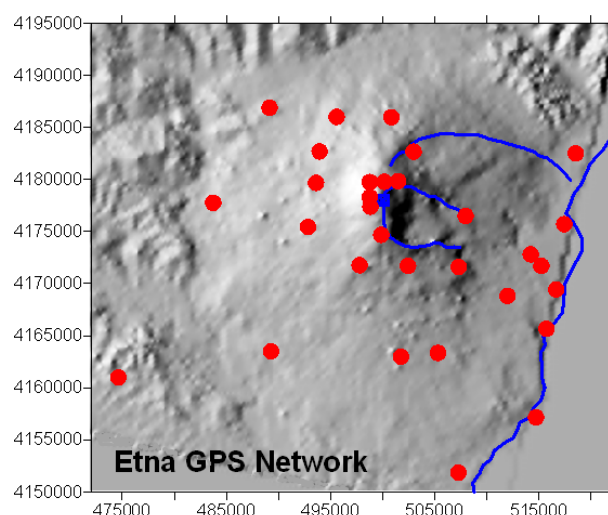
285

286   ***Figure 10.*** *Location of a network of 31 permanent GPS stations close to Mount Etna volcano*

287 *(Sicily, Italy). UTM coordinates are indicated.*

288   We analyse the three component (Up, EW, NS) deformation data corresponding to 8 successive

289   fortnightly periods, from May/2007 to September/2007 (Cannavò et al., 2015b). The data are arranged

290   into sequential files, one for each period or epoch, containing the deformation at the network stations

291   for each period. Operatively, we could imagine receiving the data files just after finishing to collect

292   and process them in a quasi-real time manner.

293   The PAF software is applied taking into account the peculiarities of the case. The **CellsConfig.exe**

294   program suggests the following values: depth of the model top = 3131 m (above sea level), depth of

295   the model bottom = -15859 m (positive above sea level), and mean side of cells = 658 m. We accept

296   these default suggestions. Then, the resulting number of cells is 33250. Next, the program suggests the

297   usual general values for the smoothing coefficient (200) and for the pressure contrast (0.5MPa).

298   The suggested pressure value 0.5 MPa is small, and we accept it as suitable for this case

299   (deformations are not very large, and therefore causative anomalous pressure should be neither very

300   large).

301   However, in this case, for the considered monitoring network the general smoothing value 200

302   looks too small. In fact, in this case the number of data points is very reduced (31 stations), the

303   measured displacements are not large (except just in the case of eruption), and GPS data involve a

304   significant inaccuracy level (estimated about 0.1 - 0.3 cm in the fortnightly period) with respect to the

305   deformation level (displacement data scattering is about 0.3 - 0.6 cm) for the considered time periods.

306   Therefore, we need to introduce a bigger smoothing coefficient to control the high noise level and

307   avoid fictitious structures. After some trial and error running of the code we have select the value 600

308   as a suitable smoothing.

309   Then, after these selections, the inversion approach is nearly automatic. We use the usual

310   significance limit 5, and in this case we analyse 8 epochs, starting in the epoch 10 (so our data files

311   will be **D00010.txt**, **D00011.txt**, …., **D00017.txt**). The program **InverPAF.exe** takes only some

seconds to carry out the inversion for each period, and to produce the drawings and the respective output files.

Usually, the displacement results from the monitoring network, for most of the deformation periods without an eruptive episode, do not show a significant deformation. However, we have selected a particular sequence of fortnightly periods (8 successive fortnightly periods, from May/2007 to September/2007) that shown an apparent intrusive episode. See Cannavò et al. (2015) and references therein. Figure 11 shows some pictures (coming from the program display) of the resulting model for the sequential study. We can observe some features. For initial epochs (e.g. epochs (a) and (b)), the model does not show significant pressure cells (red, for pressure increase, or dark blue, for pressure decrease). There are many filled cells, but in non-significant locations (yellow or light blue) (low-sensitive cells), which look artefact sources, and are introduced by the inversion program to model some global noisy pattern.

For the next epochs, (c) to (f), we appreciate the appearance of a significant body of high pressure. It ascends in the central zone with a certain inclination towards the east, reaching a minimum depth about 3 km below sea level. This structure is similar to that modelled in Cannavó et al. (2015). In addition, we appreciate a previous alignment of deep positive (but non-significant) cells from the west to the base of the significant body. Green cells in the figure indicates cells from the previous epoch, allowing to follow the evolution of the anomalous structures from one to another epoch.

Epochs (g) and (h) return to the non-significant values of pressure changes. For epoch (h), the program detects and reject an outlier observation data (denoted with red colour in the corresponding data panel in Figure 11).
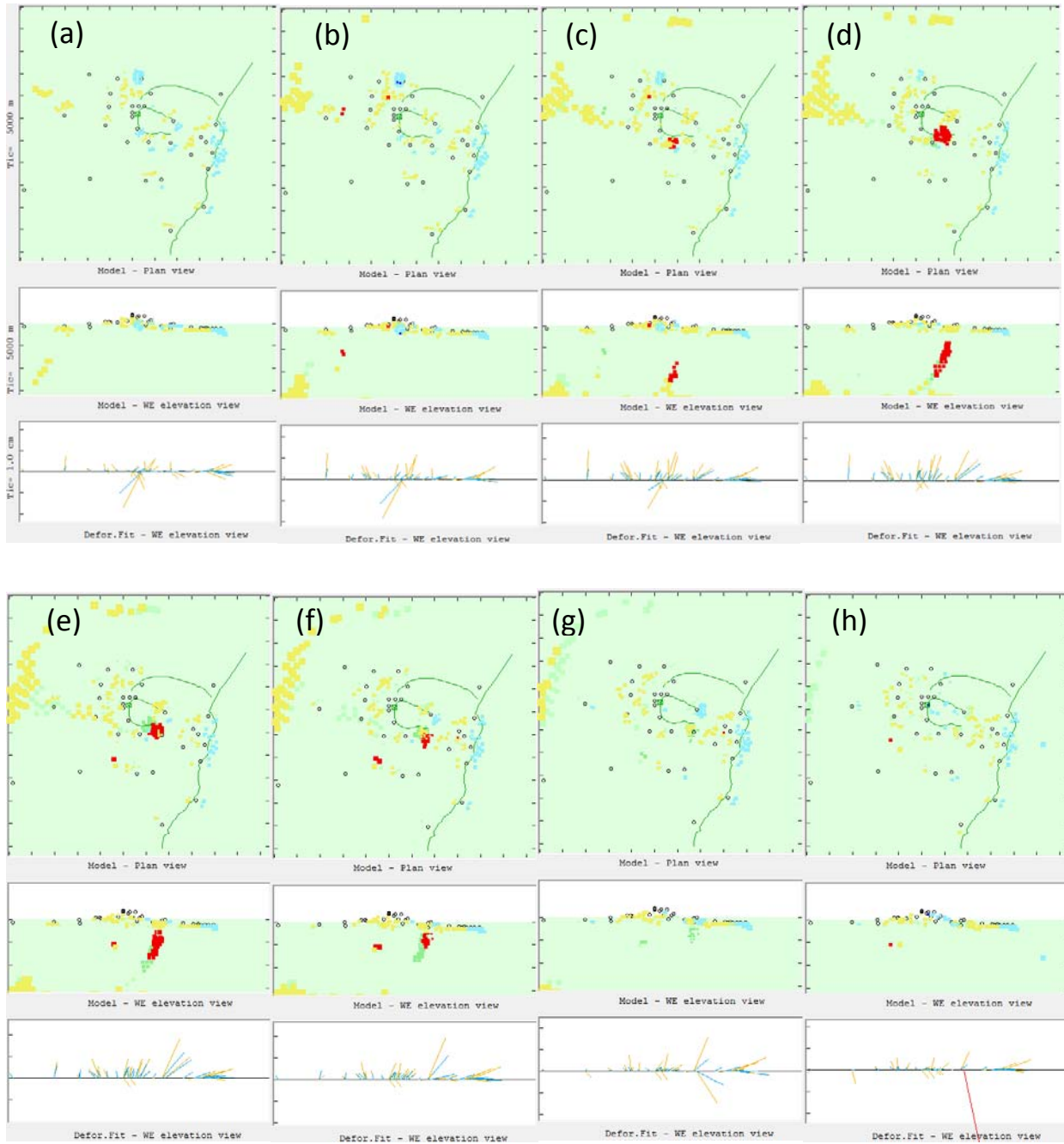
19

333

334

Figure 11. *Planar and WE elevation views of the successive inversion models obtained in the sequential monitoring for the Etna network (biweekly data, from May to September 2007). Yellow and light blue cells indicate non-significant cells (fictitious structures to absorb data distortions). Epochs (c) to (f), with a significant high pressure body (red colour), suggest an intrusive episode. Tic step in axes correspond to 5 km.*

4. Conclusions

PAF software allows carrying out an inversion, in a nearly automatic mode, of displacement data (1D to 3D) as extended 3D sources of overpressure bodies with free geometry. An elastic half-space response in assumed for the deformation calculus for each elementary source. The source bodies are described as aggregation of small cells filled with the prescribed pressure contrast. It works properly for volcanic areas, where deformations can be supposed as (mainly) due to subsurface pressure sources.

The software requires to be tuned by choosing suitable values for two main parameters in the inversion approach: the smoothing coefficient λ (which controls the balance between data fit and model regularity in the regularity conditions) and the basic pressure contrast (in MPa). Suitable values for both parameters are normally selected in a trial and error way, looking for good model features (regularity, size, etc.) and good residual distribution (null autocorrelation of residuals). Nevertheless, the choice of these parameters is not too critical with respect to the main features of the resulting model.

As shown in the application examples, the software can work for large data sets (for instance, coming from InSAR data), and for reduced sets of sequential data (for instance, coming from a small GPS monitoring network). It can work for fully 3D data, or also for 1D or 2D data (using e.g, GNSS, InSAR, or levelling data). For both application examples, geometry of the resulting models offers interesting features to evaluate the deformation causative phenomenon.

This software consists of two executable programs, and can be freely downloaded from the web page of the journal or asking to the corresponding author. The first program (**ConfigPAF.exe**) allows the user to set (in a dialog mode) the values for the inversion parameters, and for the geometrical configuration of the small cells. The second program (**InverPAF.exe**) works with the results of the former program, and does not require any user involvement (display of intermediate or final result is optional). It can be incorporated into a larger software tool for monitoring at a volcanic observatory

21

364 and even can run in an automatic way in real time, giving also very useful results (see Cannavò et al.,

365 2015). The source codes, user manual, executable files and a test example (including input data and

366 results) can be obtained on request to the corresponding author, under an open source license.

371 **References.**

372 Allard, P., Behncke, B., D'Amico, S., Neri, M., and Gambino, S. (2006) Mount Etna 1993–2005:

373   anatomy of an evolving eruptive cycle, Earth-Sci. Rev., 78, 85–114,

374   doi:10.1016/j.earscirev.2006.04.002.

375 Aloisi, M., Bonaccorso, A., and Gambino, S. (2006) Imaging compositive dike propagation (Etna,

376   2002 case), J. Geophys. Res., 111, B06404, doi:10.1029/2005JB003908.

377 Battaglia, M., and Hill, D.P. (2009), Analytical modeling of gravity changes and crustal deformation

378   at volcanoes: The Long Valley caldera, California, case study, Tectonophysics, 471, 45-57, doi:

379   10.1016/j.tecto.2008.09.040.

380 Branca, S., Coltelli, M., and Groppelli, G. (2011) Geological evolution of a complex basaltic

381   stratovolcano: Mount Etna, Italy, Ital. J. Geosci., 130, 306–317, 2011. doi: 10.3301/IJG.2011.13.

382 Camacho, A. G., González, P. J., Fernández, J., & Berrino, G. (2011) Simultaneous inversion of

383   surface deformation and gravity changes by means of extended bodies with a free geometry:

384   Application to deforming calderas. *J. Geophys. Res.*, 116, B10401. doi.org/10.1029/2010JB008165

385 Camacho, A. G., J. C. Nunes, E. Ortiz, Z. França, and R. Vieira (2007), Gravimetric determination of

386   an intrusive complex under the Island of Faial (Azores): Some methodological improvements,

387   *Geophys. J. Int.,* 171, 478–494, doi:10.1111/j.1365-246X.2007.03539.x.

388 Cannavó, F., Arena, A., & Monaco, C. (2015a). Local geodetic and seismic energy balance for shallow

389   earthquake prediction. Journal of Seismology, 19(1), 1-8, doi:10.1007/s10950-014-9446-z.

390 Cannavò, F.; Camacho; A.G.; González, P.J.; Mattia, M.; Puglisi, G; and Fernández, J. (2015b) Real

391   Time Tracking of Magmatic Intrusions by means of Ground Deformation Modeling during

392   Volcanic Crises, Scientific Reports, 5:10970. doi: 10.1038/srep10970

393 Charco, M., Fernández, J., Luzón, F., Tiampo, K.F., and Rundle, J.B. (2007), Some insights into

394   topographic, elastic a self-gravitation interaction in modelling ground deformation and gravity

395   changes in active volcanic areas, *Pure Appl. Geophys.*, 164, 865-878, doi 10.1007/s00024-004-

396   0190-y

397 Dzurisin D. (2003), A comprehensive approach to monitoring volcano deformation as a window on

398   the eruption cycle, Rev. Geophys., 41(1), 1001, doi:10.1029/2001RG000107.

399 Lisowski, M. (2007), Analytical volcano deformation source models, in Volcano Deformation, chap.

400   8, pp. 279-304, Springer Praxis, Chichester, U.K.

401 Mogi, K. (1958) Relations between the eruption of various volcanoes and the deformation of the

402   ground surface around them. *Bull. Earthquake Res. Inst. Univ. Tokyo*, 36, 99-134.

403 Rymer, H and Williams-Jones, G. (2000). Volcanic eruption prediction: Magma chamber physics from

404   gravity and deformation measurements. Geophys. Res. Lett., 27-16, 2389-2392. doi:

405   10.1029/1999GL011293

406 Samsonov, S. V., Tiampo, K. F., Camacho, A. G., Fernández, J., and González, P. J. (2014)

407   Spatiotemporal analysis and interpretation of 1993–2013 ground deformation at Campi Flegrei,

408   Italy, observed by advanced DInSAR. *Geophys. Res. Lett.*, 41, 6101–6108 (2014). doi:10.1002/

409   2014GL060595.

410   Willians, C.A., and Wadge, G. (1998), The effects of topography on magma chamber deformation

411   models: Application to Mt. Etna and radar interferometry, Geophys. Res. Lett., 25, 1549-1552.